MEBT-BI-WS02-04

Thermo-Mechanical Analysis of MEBT Wire Scanner

A. R. Páramo A. Vizcaíno Z. Izaola I.Bustinduy

19 June 2017

Project: MEBT
Version: 0.4
Approved by: I. Bustinduy
Revised by: Z.Izaola, A. Vizcaino

Change History

Rev.	Date	Author(s)	Description
0.1	2016-11-07	A. R. Páramo	First Version
0.2	2016-12-14	A. R. Páramo	Second Version. An analytical model is included and the FEM model is updated in order to simulated all irradiation pulses.
0.3	2016-12-23	A. R. Páramo	Tungsten Wire Analysis included as an appendix. The analysis is done for MEBT Wire Scanners and EMU/Grid. Beam operational limits for Wire Scanners and EMU/Grid are included as an appendix.
0.4	2016-06-19	A. R. Páramo	Minor modifications. The appendix with the analysis of EMU/Grid wires has been taken out as a separate report.

Thermo-Mechanical Analysis of MEBT Wire Scanner

A. R. Páramo[1*], A. Vizcaino[1], I. Bustinduy[1]

[1] Accelerator/Control & Diagnostics Group, ESS-Bilbao, Spain

[*]Corresponding author: arparamo@essbilbao.org

1. Introduction

Three Wire Scanners will be installed in the ESS MEBT Line in order to measure the transverse beam profile. In Figure 1 we show the position and beam size in the MEBT for the three Wire Scanners [1, 2].

The wire scanners will operate in the commissioning mode [3] with a beam energy of 3.63 MeV, currents of 62.5 mA, pulse duration of 50 μs and repetition rates of 1 Hz. The wires are made of carbon with diameters of 33 μm and lengths of 76 mm.

Previous analysis of carbon wires can be found in Ref. [4] for SNS or in Refs. [2, 5] for ESS[1]. In Ref. [2] it is specified that the maximum temperature for the carbon wires should be below ≤ 2000 K in order to avoid carbon sublimation. Also, in the range of 1500-2000 K, special attention should be paid to thermionic emission. In this work we update the results of Refs. [2, 5] in order to agree with the final operational parameters expected in the ESS MEBT. In Table 1 the main operational parameters the MEBT wire scanners are summarized.

[1] The analysis for the ESS Wire Scanner in Refs. [2, 5] cover a broad range of irradiation energy, from the MEBT (3.63 MeV) up to 2000 MeV. In the case of the MEBT the parameters of the analysis are different from the reported in this work, with different pulse duration and beam sizes.

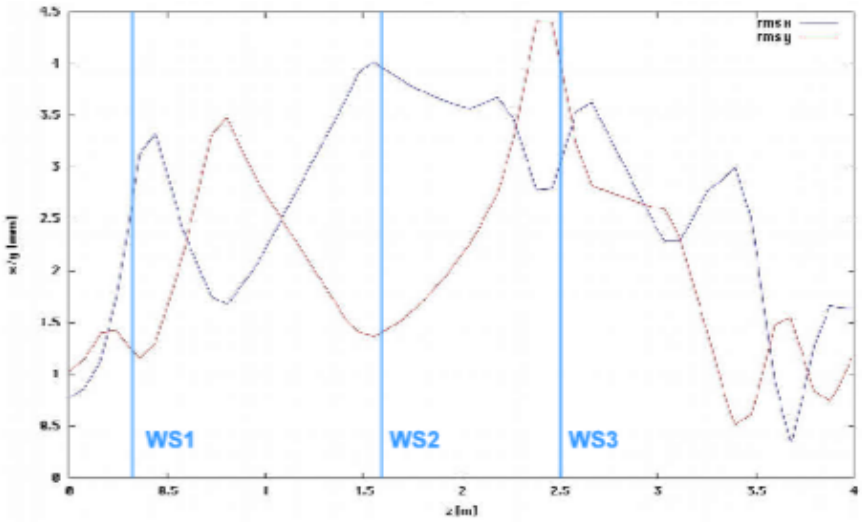

Figure 1: Beam size in the MEBT and in the position of the three Wire Scanners. Figure from Ref. [1].

Table 1: Main parameters of the model

Parameter	Value		Parameter		Value	
Proton Energy	3.63	MeV	WS1	σ_x	2.43	mm
Intensity	62.5	mA		σ_y	1.277	mm
Irradiation Mode	50 μs - 1 Hz		WS2	σ_x	3.923	mm
				σ_y	1.432	mm
Wire Diameter	33	μm	WS3	σ_x	3.157	mm
Wire Length	76	mm		σ_y	3.835	mm

2. Model Description

2.1. Thermal Load

The thermal load in the wire scanner is calculated from simulations in MCNPX [6], SRIM [7] and values reported by NIST database [8].

In the case of graphite, the stopping power at the surface is ~160 MeV/cm. In Figure 2 the stopping power graphite is shown for MCNPX and SRIM simulations for graphite densities of ρ=1.8 g/cm^3, we observe how the stopping power at the surface is ~160 MeV/cm and it keeps almost constant below the carbon wire diameter (33 μm). In the NIST data base stopping powers of ~90 MeV-cm^2/g are given, which for densities of ρ=1.8 g/cm^3 also means stopping powers ~160 MeV/cm.

In the case of tungsten the stopping power at the surface is ~660 MeV/cm. In Figure 2 the stopping power for tungsten is shown for MCNPX and SRIM simulations for graphite densities of ρ=19 g/cm^3, we observe how the stopping power at the surface is ~660 MeV/cm. In the NIST data base stopping powers of ~34 MeV-cm^2/g are given, which for densities of ρ=19 g/cm^3 also means stopping powers ~660 MeV/cm.

The deposited heat by a beam irradiation, $\dot{q}$, can be calculated as the multiplication of the stopping power S (MeV/cm) by the current density I'' (mA/cm^2):

$$\dot{q} = S \cdot I'' = S \cdot \frac{I_0 \cdot e^{-\left(\frac{x^2}{2\sigma_x^2}+\frac{y^2}{2\sigma_x^2}\right)}}{2 \cdot \pi \cdot \sigma_x \cdot \sigma_y} \quad (1)$$

Where I_0 is the beam current and σ the beam size.

In Figure 3 the heat deposition for the different carbon wire scanners is shown, the maximum heat load is obtained for the WS1H with ~50 MW/cm^3.

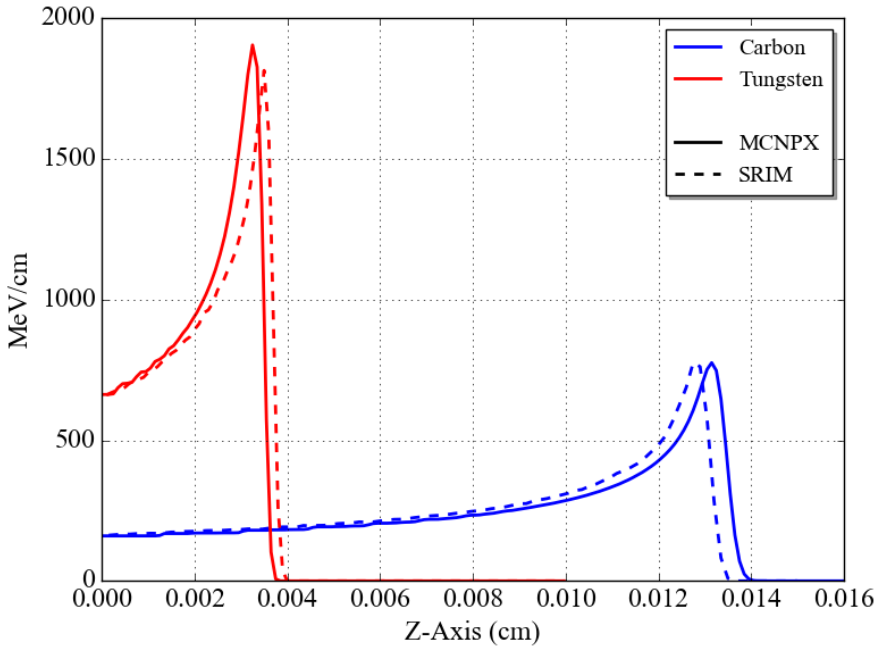

Figure 2: Stopping power for 3.63 MeV protons in Graphite (blue) and tungsten (red), comparison of MCNPX and SRIM models.

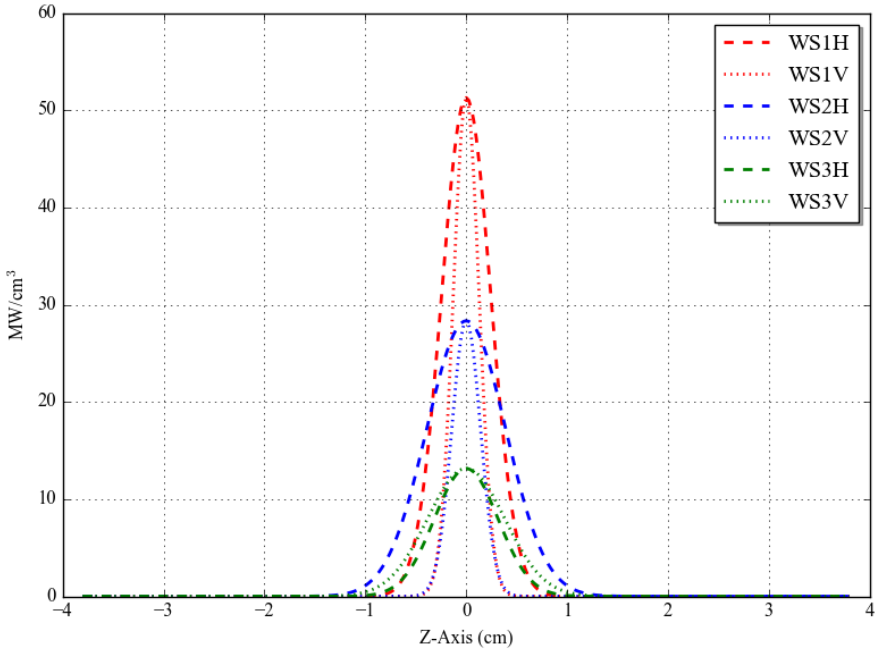

Figure 3: Heat deposition in the different Wire scanner positions for the ESS MEBT 3.63 MeV proton beam.

2.2. **Analytical Model**

An analytical model is developed in order to have quick estimations of irradiation effects on the carbon wire and as a mean to validate more detailed FEM models.

In the analytical model we calculate the temperature in the wire scanner from heat balance.

The general expression for heat equation is:

$$\rho \cdot c_p \cdot \frac{\partial T}{\partial t} - \nabla \cdot (k \nabla T) = \dot{q} \tag{2}$$

Where ρ is the density, c_p the specific heat capacity, T the temperature, t the time, k the thermal conductivity and $\dot{q}$ the heat deposition from beam irradiation.

For an analytical model, neglecting thermal conductivity we have a 0D equation:

$$\rho \cdot c_p \cdot \frac{\partial T}{\partial t} = \dot{q} \tag{3}$$

In order to perform the heat balance, we apply the 0D heat equation in a differential control volume. The control volume is defined with the wire radius r and a differential length dL, for a volume ($V = \pi r^2 \cdot dL$) and an external area ($A=2\pi r \cdot dL$). The heat balance in the control volume is:

$$\underbrace{\rho \cdot c_p \cdot V \cdot \frac{\partial T}{\partial t}}_{Wire\ Heating} = \underbrace{\dot{q} \cdot V}_{Beam\ Irradiation} - \underbrace{\dot{A} \cdot \epsilon \cdot \sigma \cdot (T^4 - T_0^4)}_{Radiative\ Heat} \tag{4}$$

$$\frac{\partial T}{\partial t} = \frac{\dot{q}}{\rho \cdot c_p} - \frac{A}{V} \cdot \epsilon \cdot \sigma \cdot (T^4 - T_0^4) \tag{5}$$

Also the ratio A/V, can defined by the wire radius r:

$$\frac{A}{V} = \frac{2\pi \cdot r \cdot \mathrm{d}L}{\pi \cdot r^2 \cdot \mathrm{d}L} = \frac{2}{r} \tag{6}$$

Therefore Eq. (5) can be simplified to:

$$\frac{\partial T}{\partial t} = \frac{\dot{q}}{\rho \cdot c_p} - \frac{2}{r} \cdot \epsilon \cdot \sigma \cdot (T^4 - T_0^4) \tag{7}$$

2.3. **FEM Model**

In order to include thermal diffusion, an Ansys FEM model [9] is used. In the Ansys model a 1D approach is used. In the model the wire is represented by 1D beam elements and irradiation trough irradiation elements to an ambient node at 300 K. Regarding the mechanical constraints, we impose them depending on the wire condition (tensile or loose). For a tensile conditions, we evaluate the stress variation assuming that wire sides are fixed. For a loose wire we calculate wire deformation in assuming free movement on one side of the wire.

In Figure 4 we show an scheme with the main components of the 1D FEM model of the wires.

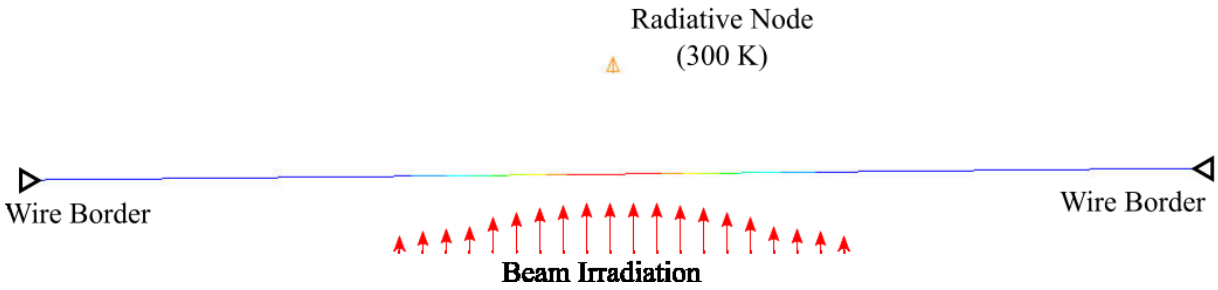

Figure 4: Scheme showing the main components of the wires 1D FEM model.

3. Results

3.1. Carbon Wire Temperature

In this section we present the results using the Ansys FEM for the different Wire Scanner of the MEBT.

During operation in the MEBT, the carbon wires will be irradiated. Irradiation will lead to wire heating during the pulse duration, and cooling down due to thermal radiation in between pulses.

In Figure 5 we show the temporal evolution of the temperature in the wire scanner (WS1H). We compare the analytical and Ansys FEM model. In the case of FEM model, there is heat dissipation through heat conductivity along the wire. The axial heat conductivity leads to temperatures ~100 K lower than in the analytical model.

Regarding the temperature evolution, it is observed that a steady state is attained in just a few pulses. Then the pulse transients heats up the wire during the pulse duration (50 μs) and the wire cools down after the pulse.

In Table 2 we show the temperature in for the MEBT wire scanners in the different positions. Since the wire scanner 1 (WS1) has the smaller beam size, the beam focusing will lead to higher temperatures, that lead to higher thermal force and deformations. The position of the wire scanner also affects the temperature, in the case of the Wire Scanner 1, in Horizontal (WS1H) position more beam irradiates the wire ($\sigma_x > \sigma_y$) leading to higher temperatures.

In Figure 6 we show the temperature profile after the irradiation pulse for the different wire positions. We observe how the temperature is directly dependant on the beam irradiation. For the different cases the wire is hotter in the centre and cools down to the sides, with the temperature profile following a distribution similar to the Gaussian beam irradiation profile (see Figure 3). Comparing the different cases, the WS1H scenario shows the higher temperature due to its higher beam irradiation.

Table 2: Temperature, force and deformation for the MEBT wire scanners in Vertical (V) and Horizontal (H) position.

Case	T_{steady} (K)	T_{peak} (K)	F (N)	$\Delta\sigma$ (MPa)	ΔL (μm)
WS1H	531	1363	0.009	10	65
WS1V	476	1323	0.006	7	44
WS2H	527	1024	0.008	10	63
WS2V	439	962	0.004	5	33
WS3H	442	713	0.005	5	35
WS3V	458	725	0.005	6	40

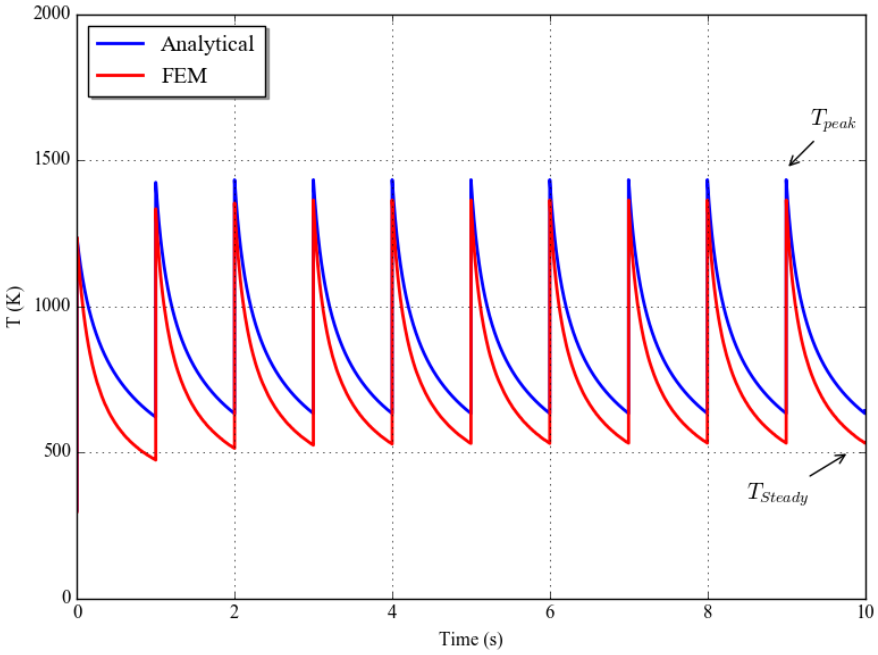

Figure 5: Temperature evolution for WS1H comparing the analytical (blue) and FEM (red) models.

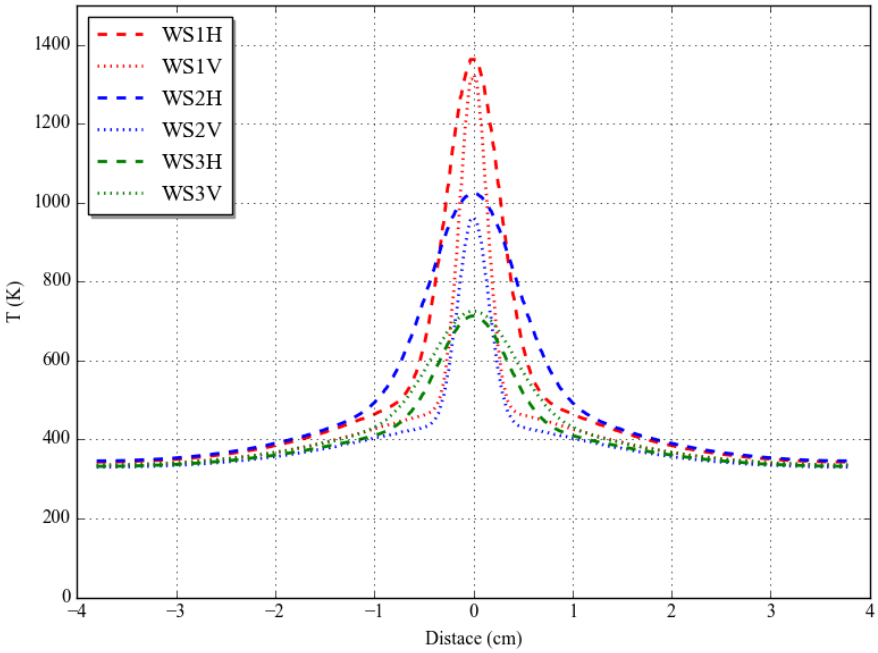

Figure 6: Temperature profile along the wire after the irradiation pulse. The different wire positions are shown, red for WS1, blue for WS2 and green for WS3 in dashed lines Horizontal positions and in dotted lines Vertical positions. The figure shows the results obtained with the FEM model.

3.2. **Mechanical Effects**

Regarding mechanical behaviour, in order to compensate thermal expansion, an initial preload will be applied to the wire. Therefore, before the pulse arrival, the wire will be in a tensile state. During the pulse, thermal expansion will reduce the tensile stresses in the wire or will bend the wire depending on the preload. If the preload is higher than the thermal expansion, the wire will keep its tensile condition. On the contrary, if the preload is lower than the thermal expansion, the wire will bend leading to transverse deformation.

If the preload is lost during operation, axial deformations will appear (ΔL). This deformation will bend the wire leading to transverse deformations (Δy). Using trigonometry we can calculate the transversal deformation Δy, see Figure 7 and Eq. (8)

$$\Delta y = \frac{\sqrt{2 \cdot \Delta L \cdot L + \Delta L^2}}{2} \qquad (8)$$

Therefore, in order to avoid wire bending, we need to guarantee operation in a tensile state. This means that the wire preload has to be higher than the force induced by thermal expansion.

In Table 2 we observe that the force induced by thermal expansion is at most of ~0.01 N leading to stress variations of $\Delta\sigma$ ~10 MPa. The thermal expansion of ~0.01 N could be compensated with an equivalent preload, which means that a preload of at least 1 g should be guaranteed.

For a nominal length of L=76 mm and an axial deformation ΔL~65 μm (see Table 2), a transversal deformation of Δy~1.6 mm appears. Therefore, even small axial deformation can lead to large transversal errors. It is important to guarantee that the wire keeps its tensile stress conditions at any point of operation.

Regarding the structural integrity of the wire, in principle preloads of ~20 g are going to be applied, which exceeds the minimum of 1g estimated in this work. For a preload of 20 g (0.196 N) in a wire of 33 μm of diameter, tensile stresses of 230 MPa are induced. The wire strength should be assessed and in order to avoid fatigue appearance due to cyclic loading, it is recommended to design the carbon wire to operate with stresses below 50% of the tensile strength [10–12].

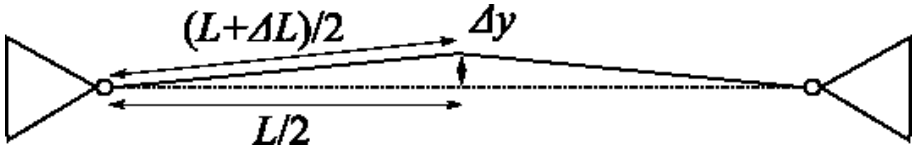

Figure 7: Deformed wire, where L is the original distance, ΔL the length increase, and Δy the transversal deformation.

4. **Conclusions**

We have studied the maximum temperatures, thermal force, and possible deformation for the wires of the MEBT wire scanners.

We conclude that the maximum temperatures are below 1500 K. Below 1500 K correct operation of the carbon wire is expected, with no thermionic emission or carbon sublimation effects.

Regarding thermal expansion, we conclude that a preload of at least 1 g (0.01 N) needs to be effectively applied. In general, it is important to guarantee that the preload guarantees the tensile condition, and the wire does not get loose during operation. If the wire loses its tensile condition, large transversal deformation is expected, on the order of mm.

Appendix A: Material Properties

In this model we use Graphite R4550 and tungsten material properties obtained from Linac 4 Cern Group, and reported in Refs. [13–15].

For the carbon filament we take an emissivity of ϵ=0.53 [16]. This value is taken as a conservative estimation, other reported values point to emissivities ~0.8 [4, 5]. For the tungsten filament we take an emissivity of ϵ=0.1 [5]. This value is taken as a conservative estimation, other reported values point to emissivities for tungsten filament ~0.3 [16].

The material properties of the materials used in the work are summarized in Table 3.

Table 3: Material properties for Graphite R4550 and tungsten [13, 14] .

Mat. Limit	**Graphite**	**Tungsten**
Max. Temp. (K)	3773	3673
Young Modulus (GPa)	11.7	405
Poisson Coefficient	0.15	0.3
Thermal Conductivity at 300 K (W m^{-1} K^{-1})	103	173
Density at 300 K (kg m^{-3})	1800	19000
Specific Heat at 300 K (J kg^{-1} K)	824	133
Coefficient Of thermal expansion at 300 K (μm/m)	4	5

Appendix B: Analytical Model Validation

The analytical model described in Section 2 is implemented in Python and Octave programs. Furthermore we have developed an Ansys model (Ansys 0D) that reproduces the analytic results. For this purpose we neglect conductivity in the Ansys FEM model.

In Figure 8 we show the temperature evolution for the different models. In particular we study the case of the Wires Scanner 1 in Horizontal position (WS1H). As expected all the 0D models, that solve Eq. (7) offer the same results. In Table 4 we show the final temperature values for the different models.Only small differences appear, that are due to small errors in the numerical solver.

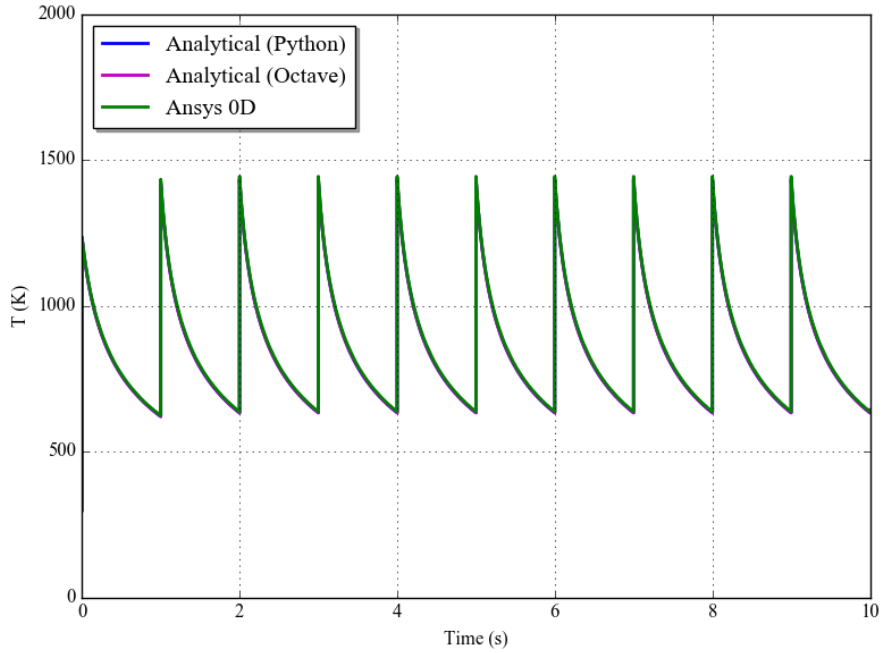

Figure 8: Temperature evolution for WS1H assuming different models that neglect axial thermal conductivity.

Table 4: Temperatures in the MEBT WS1H for different models: analytical (python, octave) and FEM (Ansys 0D, Ansys 1D).

Model	Tpeak (K)	Tsteady (K)
Python	1432	632
Octave	1430	633
Ansys 0D	1443	637

Appendix C: Analytical Model Comparison with ESS Cheymol's Analysis

In this section we compare the analytical model presented in Section 2 with the results presented by B. Cheymol in Ref. [5]. It is important to point out that in Ref. [5] different irradiation conditions to the presented in this work as used. Therefore for the comparison we use the irradiation conditions of Ref. [5] with pulse duration of 100 µs, beam size of σ_x = 1.85 mm, σ_y= 1.45 mm and an emissivity ϵ=0.8. Also the material properties may slightly differ since in Ref. [5] material properties are obtained from pyrolytic carbon of Ref. [17].

Obseving Figure 9 we verify that both models attain similar results, with peak temperatures ~2250 K.

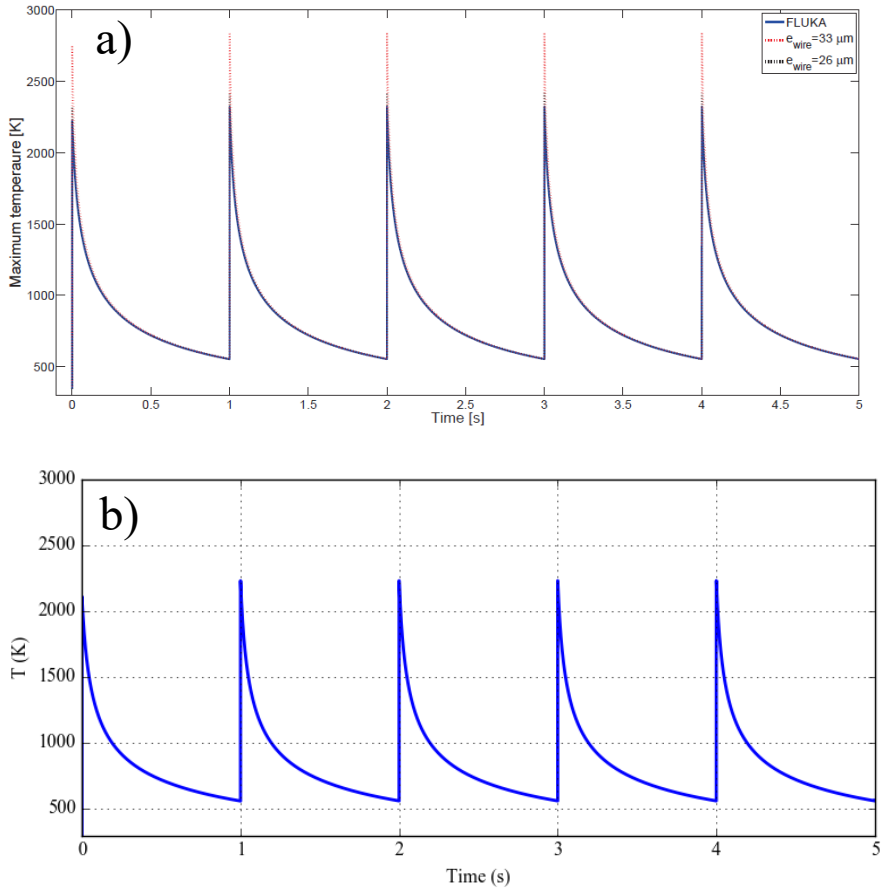

Figure 9: Model comparison for Carbon Wire temperature, results with parameters from Ref. [5]: t=100µs, ϵ=0.8, , σ_x = 1.85, σ_y=1.45. a) Figure from Ref. [5] b) Calculations with the model pres4ented in this work.

Appendix D: Tungsten Wire Analysis

In this section we assess if tungsten wires could be used in the Wire Scanners to replace the carbon wires.

We study tungsten wires with diametres of 33 μm. For the results obtained in this section, we use the Analytical and FEM models described in Section 2. The thermal load in tungsten results from stopping powers[2] ~660 MeV/cm (see Section 2.1). The tungsten material properties are defined in Appendix A: Material Properties.

In Figure 10 we show the temperature of the tungsten wire with the analytical and FEM model in the WS1H position. We observe that the peak temperature is in all cases higher than 4000 K, which exceeds tungsten melting temperature. Therefore tungsten wires cannot be used in the MEBT, for protons of 3.63 MeV and stopping powers ~660 MeV/cm.

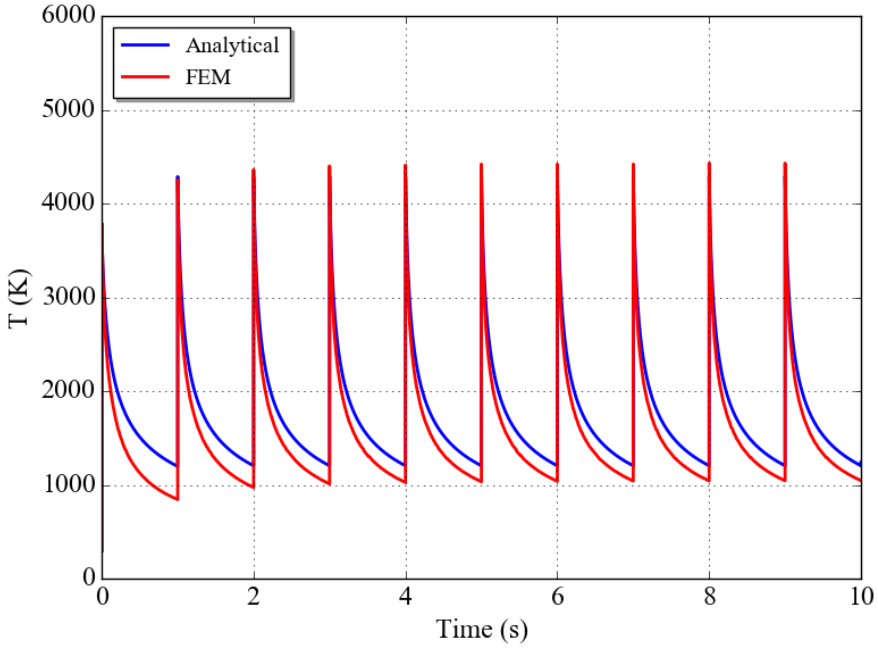

Figure 10: Temperature evolution for a tungsten wire in WS1H comparing the analytical (blue) and FEM (red) models.

[2] 660 MeV/cm is the stopping power for 3.63 MeV in the surface. For tungsten wires of >20 μm of diameter the average stopping power is higher due to the appearance of the Bragg peak. Therefore the presented calculations underestimate the temperature increase in the tungsten wire.

Appendix E: Operational Limit for MEBT Wire Scanner

In this work we have estimated the wire operational conditions under the nominal beam parameters. However during commissioning phase the beam parameters will be tuned until the nominal mode is attained. Therefore if the beam get focused or its pulse duration increases, high thermal loads may appear which may result in damage of the MEBT wires. In order to avoid operation in non-desired scenarios we define an operational limit though the use of the integrated current density, I_c.

During irradiation the temperature variation is directly related to the heat deposition ($\dot{q}$):

$$\rho \cdot c_p \cdot \frac{\partial T}{\partial t} = \dot{q} = S \cdot I'' = \frac{I_0}{2\pi\sigma_x\sigma_y} \cdot S \cdot \quad (9)$$

Assuming constant properties, integrating during the pulse duration τ, the pulse the temperature is:

$$T_{peak} = T_{steady} + \underbrace{\frac{S}{\rho \cdot c_p}}_{\substack{Material \\ Properties}} \cdot \underbrace{\frac{I_0}{2\pi\sigma_x\sigma_y} \cdot \tau}_{\substack{Beam \\ Parameters}} \quad (10)$$

Therefore the maximum temperature depends on the material properties and the beam parameters. In order to define the limit for operation we can define an operational limit with the integrated current density (I_c):

$$I_c = \frac{I_0}{2\pi\sigma_x\sigma_y} \cdot \tau \quad (11)$$

Using the analytical model described in Section 2.2, we have estimated the maximum temperature in the wire as function of I_c.

In order to define an operational limit we define:

- Limit 1: thermionic emission at 1500 K [2]. Operation above this limit will introduce signal noise due to thermionic emission and damage effects on the wire may begin to appear. For temperatures between 1500-3000 K, carbon wires will begin to sublimate [2] and tungsten wires will suffer from annealing and recrystallization effects.
- Limit 2: maximum operational temperature 3000 K. Above this temperature the wires will most probably be damaged.

In Figure 11 we show the maximum temperature in the MEBT wires as function of I_c. In Table 5 we give the I_c limits for carbon and tungsten wires. With carbon wires correct operation will be possible in all cases. Wire tungsten could not be installed in the wire scanner or they would destroyed.

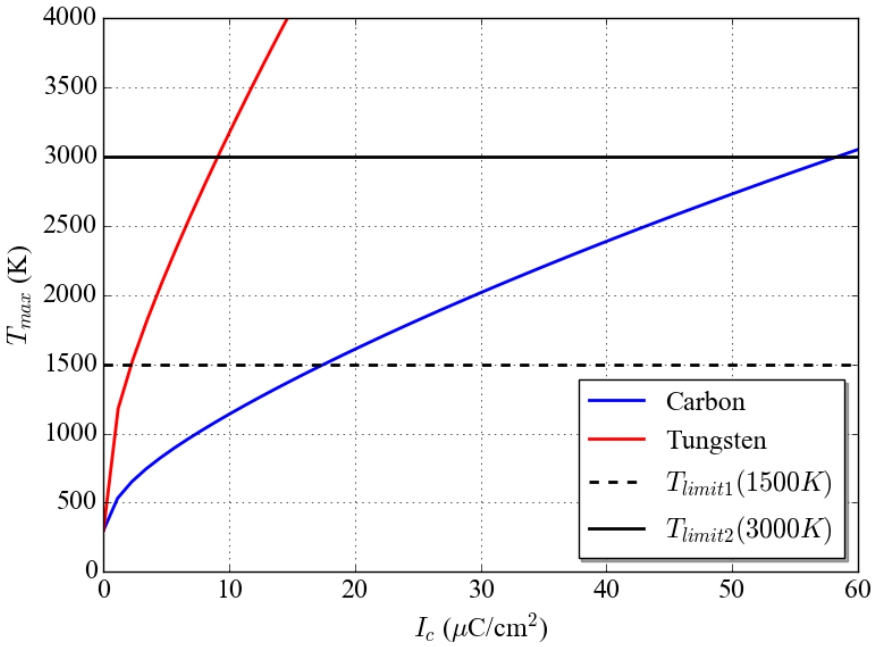

Figure 11: Temperature in the wire as function of integrated current density I_c. The curves are obtained using the analytical model.

Table 5: Integrated current density I_c limits for carbon and tungsten, and operational values expected in the different wires of the MEBT. The limits are obtained using the analytical model.

	I_c (μC/cm^2)
Limit 1 Carbon (T=1500 K)	17
Limit 2 Carbon (T=3000 K)	58
Limit 1 Tungsten (T=1500 K)	2
Limit 2 Tungsten (T=3000 K)	9
WS1	16.0
WS2	8.9
WS3	4.1

References

[1] D. Vizcaíno, “Wire Scanner Mechanical Design Concept,” Jul-2016.

[2] B. Cheymol and A. Jansson, “European Spallation Source wire scanner conceptual design,” Internal ESS ESS-0020237, Nov. 2014.

[3] M. Munoz, M. Eshraqi, A. Jansson, S. Molloy, and M. Lindroos, “Description of Modes for ESS Accelerator Operation,” Internal ESS ESS-0038258 Rev. 3 Prelminary State, Nov. 2015.

[4] C. J. Liaw and P. R. Cameron, “Carbon wire heating due to scattering in the SNS,” in *Particle Accelerator Conference, 2001. PAC 2001. Proceedings of the 2001*, 2001, vol. 3, pp. 2365–2367.

[5] B. Cheymol, “Effects of Energy Deposition Models and Conductive Cooling on Wire Scanner Thermal Load, Analytical and Finite Element Analysis Approach,” in *57th ICFA Advanced Beam Dynamics Workshop on High-Intensity and High-Brightness Hadron Beams (HB’16), Malmö, Sweden, July 3-8, 2016*, 2016, pp. 221–225.

[6] D. B. Pelowitz, “MCNPX user’s Manual Version 2.7.0,” LA-CP-11-00438, Apr. 2011.

[7] J. F. Ziegler, M. D. Ziegler, and J. P. Biersack, “SRIM – The stopping and range of ions in matter (2010),” *Nucl. Instrum. Methods Phys. Res. Sect. B Beam Interact. Mater. At.*, vol. 268, no. 11–12, pp. 1818–1823, Jun. 2010.

[8] C. Suplee, “Stopping-Power & Range Tables for Electrons, Protons, and Helium Ions,” *NIST*, 07-Oct-2009. https://www.nist.gov/pml/stopping-power-range-tables-electrons-protons-and-helium-ions.

[9] “ANSYS - Simulation Driven Product Development,” 04-Apr-2013. http://www.ansys.com/.

[10] F. Carra and A. Dallochio, “LINAC4 3MeV test stand: Thermo-mechanical fatigue analysis of the Slit,” CERN CH1211 Geneva 23 Switzerland, CERN Internal Report 1102151 0.1 DRAFT, Nov. 2010.

[11] H. Mayer and M. Papakyriacou, “Fatigue behaviour of graphite and interpenetrating graphite–aluminium composite up to 109 load cycles,” *Carbon*, vol. 44, no. 9, pp. 1801–1807, Aug. 2006.

[12] F. H. Ho, “Graphite Design Handbook,” General Atomics, San Diego, CA (US), DOE/HTGR--88111, Sep. 1988.

[13] F. Carra and A. Dallochio, “LINAC4 3MeV test stand: Thermo-mechanical analysis of the Slit,” CERN, CERN CH1211 Geneva 23 Switzerland, CERN Internal Report 1102149 0.1, Nov. 2010.

[14] SGL Group: The Carbon Company, “Specialty Graphites for the Metal Industry,” SGL Group, Commercial Brochure.

[15] T. Mora, I. Bustinduy, and F. Sordo, “ESS-Bilbao Beam Stoppers criteria (MEBT-BI-FC04-02),” 16-May-2016.

[16] Mikron Instrument Company, “Table of emissivity of various surfaces.” .

[17] “http://aries.ucsd.edu/LIB/PROPS/PANOS/.” .